Wheel–rail dynamics with closely conformal contact Part 2: forced response, results and conclusions

A Bhaskar, **K L Johnson** and **J Woodhouse**
Engineering Department, Cambridge University

Abstract: The linearized dynamic models for the conformal contact of a wheel and rail presented in reference (**1**) have been used to calculate the dynamic response to a prescribed sinusoidal ripple on the railhead. Three models have been developed: single-point contact with low or high conformity, and two-point contact. The input comprises a normal displacement $\Delta\, e^{i\omega t}$ together with a rotation $\psi\, e^{i\omega t}$ applied to the railhead. The output comprises rail displacements and forces, contact creepages and forces, and frictional energy dissipation. According to the Frederick–Valdivia hypothesis, if this last quantity has a component in phase with the input ripple, the amplitude of the ripple will be attenuated, and vice versa. Over most of the frequency range, a pure displacement input ($\psi = 0$) was found to give rise, predominantly, to a normal force at the railhead. A purely rotational input ($\Delta = 0$) caused a single point of contact to oscillate across the railhead or, in the case of two-point contact, to give rise to fluctuating out-of-phase forces at the two points. The general tenor of behaviour revealed by the three models was similar: frictional energy dissipation, and hence wear, increases with conformity and is usually of such a phase as to suppress corrugation growth. Thus the association, found on the Vancouver mass transit system, of corrugations with the development of close conformity between wheel and rail profiles must arise from some feature of the system not included in the present models.

Keywords: wheel–rail, contact, corrugation, conformity

NOTATION

See notation given in Part I of this paper (**1**).

1 INTRODUCTION

In Part I of this paper (**1**) linearized dynamic models for wheel–rail contact were developed, with the particular aim of investigating the influence of close conformity between the transverse profiles of the wheel and the rail on the generation of short-pitch corrugations. It was shown that the models did not exhibit linear instability for any reasonable combination of parameter values and degree of conformity. Those models will now be used to examine the response to a pre-existing surface ripple, from which the dynamic contact forces and frictional energy dissipation can be calculated.

Following the Frederick–Valdivia hypothesis that the rate of wear is directly proportional to the dissipation, modification of the initial ripple depends on the relative phase of the fluctuating component of dissipation. If dissipation is in phase at the ripple crests the ripple will tend to be attenuated, while if it is in phase at the troughs the ripple will be deepened. Corrugation predictions based on this wear model have been produced before (**2**), but without detailed account being taken of closely conformal contact. The main aim of the present study is to establish whether such close conformity makes a significant difference to the behaviour, which in turn might give a partial explanation for experimental observations on the Vancouver 'Skytrain' system (**3**).

Valdivia (**4**) identified three 'wear modes': (a) uniform in-phase wear across the whole railhead, giving rise to corrugation crests orthogonal to the rail; (b) anti-phase wear across the railhead giving rise to inclined crests; and (c) in-phase wear varying across the railhead in such a way as to change the conformity of the contact. To separate these wear modes in the case of a single-point conformal contact requires knowledge of the variation of frictional dissipation within the contact area, which goes beyond the scope of this contact model. However, it is possible to extract some relevant information from the authors' two-point-contact model: in this case the third wear mode is absent, but by obtaining the amplitude and phase of the frictional dissipation at the two separate contact points, the 'wear eigenvalues' associated with the two remaining modes can be obtained.

The MS was received on 18 December 1996 and was accepted for publication on 14 April 1997.

2 FORCED RESPONSE TO A SURFACE RIPPLE

2.1 Single point of contact

Computer programs have been written (in the language Matlab) to calculate the linear forced response of the various models developed in the companion paper (**1**). For the system shown in the block diagram of Fig. 8 of that reference, the input is a displacement $\Delta\, e^{i\omega t}$ applied to the centre of the contact and a rotation in the transverse plane $\psi\, e^{i\omega t}$. These two components of input are independent and their linear responses can be superposed. Values may be specified for the set of parameters determining the assumed running conditions: normal load P_0, vehicle speed V, conicity, contact centre location α, steady longitudinal and lateral creepages ξ_{x0} and ξ_{y0}, coefficient of friction μ and conformity factor K. To investigate the effect of changes in these parameters on the dynamic response a reference state has been chosen. Parameter values for this reference state are listed in Tables 1 and 2 below.

A wide range of response data can be extracted from the program: contact motion v_i'; dynamic contact forces Q_i', P'; rail forces T', N', M'; displacements w_i', ϕ; and the contact displacement $r\theta$. The authors have chosen to record in amplitude and phase the contact forces, rail displacements, contact displacement and the fluctuating power dissipation W'. Note that by the Frederick–Valdivia hypothesis (**4**, **5**), a fluctuating power dissipation with a *negative* real part (phase angle within ±90° of 180°) corresponds to corrugation *growth*. The rail ripple Δ has been determined to be positive at a crest of rail corrugation, negative in a trough. If the energy dissipation is in phase with Δ wear will act so as to reduce the crest height, while if it is in the opposite phase wear will occur preferentially in the corrugation troughs.

Table 1 Track and wheel parameters

Track	BS113A rail with concrete sleepers, rail pads and ballast
Young's modulus E (GPa)	2.07
Rail mass M (kg/m)	56
Rail profile radius ρ (m)	0.23
Equivalent continuous sleeper mass (kg/m)	150
Equivalent continuous rail pad stiffness	
Vertical k_{z1} (MN/m/m)	200 ('hard')/50 ('soft')
Lateral k_y (MN/m/m)	18 ('hard')/9 ('soft')
Ballast stiffness k_{z2} (MN/m/m)	50
Wheel radius R_1 (m)	0.46
Nominal conicity λ (rad)	1/20

Table 2 Operational parameters, values for the reference state

Load P_0 (kN)	50
Vehicle speed V (m/s)	27.8 (100 km/h)
Contact location α (rad)	0.021
Coefficient of friction μ	0.4
Steady creepages	
Longitudinal	ξ_{x0} ($\times 10^{-3}$) ±1.45
Lateral	ξ_{y0} ($\times 10^{-3}$) ±1.45
Spin	ξ_{s0} ($\times 10^{-3}$) 1.57
Conformity factor K	51
Input ripple, displacement Δ (μm)	5.0
rotation ψ (mrad)	0.33

2.1.1 *Comparison between contact models*

The output corresponding to the reference case, using the 'low-spin' and 'high-spin' contact models, is compared in Figs 1 and 2. With the exception of the power dissipation the results are very similar. The normal contact force, the rail displacements and the displacements of the contact point are almost identical for both models. It will be seen that this is because the rail rotation and the contact displacement are largely controlled by the input ripple and the impedance of the rail, which are the same in both cases. The tangential contact forces Q_x and Q_y show a similar variation with frequency, but Q_x is roughly halved in magnitude with the high-spin contact model. This is to be expected from the known effect of spin in reducing the longitudinal creep coefficients.

The predictions of the two models differ significantly only in the frictional power dissipation (Figs 1d and 2d). This is due to the omission of spin friction from the low-spin model, which was the principal reason for the introduction of the high-spin model, whose predictions in this respect should be regarded as the more reliable. Only output from the high-spin model, therefore, will be quoted in the remainder of this section.

2.1.2 *Input ripple*

As stated above, the input irregularity (ripple) takes the form of a displacement $\Delta\, e^{i\omega t}$ and angle $\psi\, e^{i\omega t}$ each of which may be applied independently. The angle ψ takes into account the variation in phase of the corrugation across the railhead, which was observed on the Vancouver mass transit system (**3**). For the same reference state to which the response of Fig. 2 applies, the input ripple angle ψ was reduced to zero; the output is presented in Fig. 3. The normal contact force P' and the vertical rail displacement w_3 remain essentially unchanged, but the tangential contact forces, the rail rotation and contact displacement are reduced by about an order of magnitude, and the dissipation by a factor of between 2 and 3.

A case was also run in which the angle ψ was kept at the reference value of 0.33 mrad while the displacement $\Delta = 0$. The normal contact force P' and rail displacement w_3 reduced by a factor of 10, while the tangential forces, rail rotation and contact displacement remained close to the values shown in Fig. 2. The output for this case, which is simply a linear combination of those of Fig. 2 and Fig. 3, is not reproduced here.

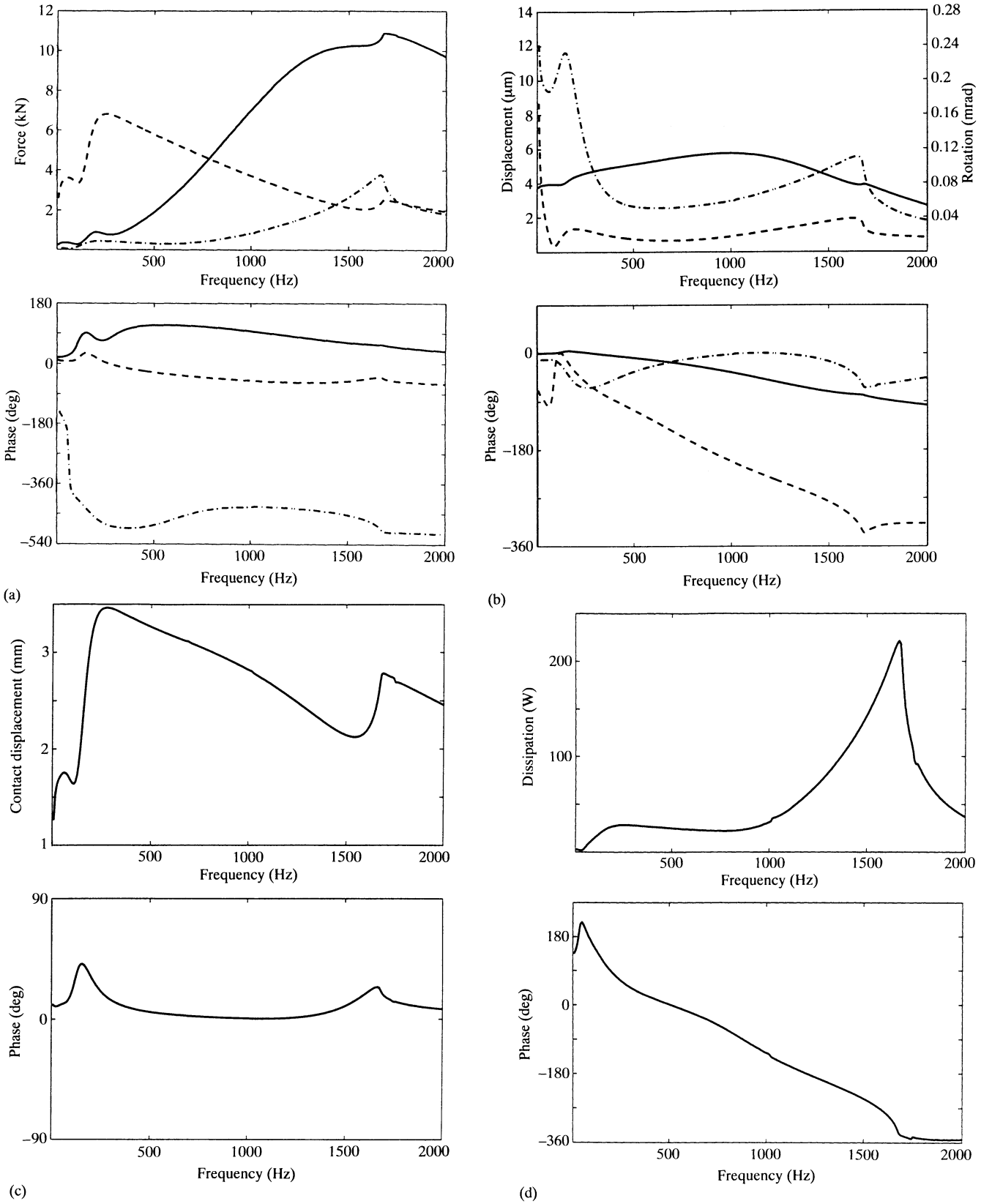

Fig. 1 Forced response results using the low-spin contact model, plotted as amplitude and phase frequency response curves: (a) contact forces (solid line: P', dashed line: Q'_x, dash-dot line: Q'_y); (b) rail displacements (solid line: vertical w_2, dashed line: horizontal w_3) and rotation ϕ (dash-dot line); (c) contact displacement $r\theta$ (d) frictional power dissipation W'. Parameter values for this reference state are given in Tables 1 and 2

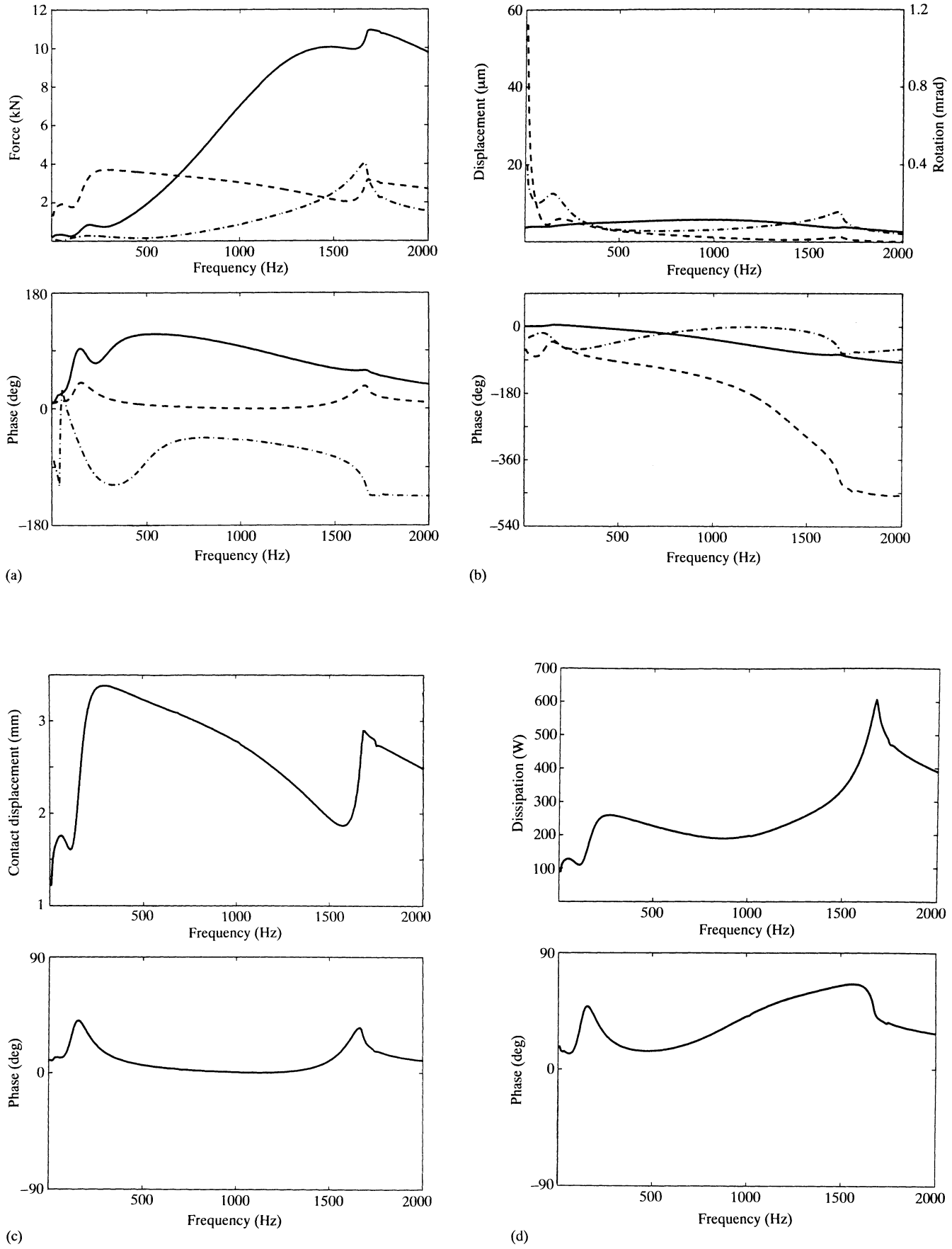

Fig. 2 Results corresponding to Fig. 1, obtained using the high-spin contact model

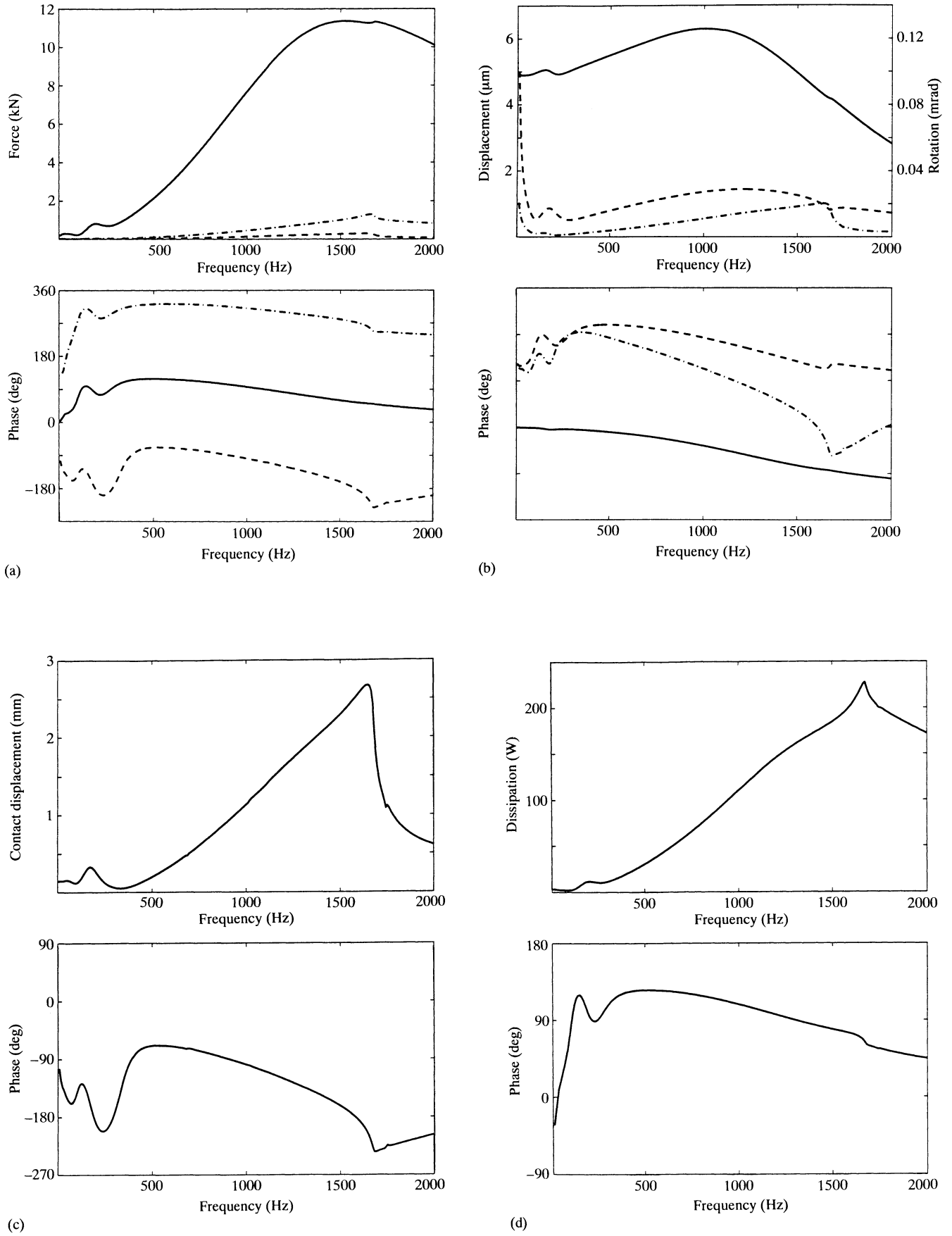

Fig. 3 Results from a run identical to that producing Fig. 2, except with $\psi = 0$

2.1.3 *Frequency response*

All the output data are plotted as a function of frequency. The frequency response is governed by the rail receptances shown in Fig. 4 of the companion paper (**1**). Thus a constant input displacement, together with the decrease of vertical receptance H_{33}, is responsible for the increase in normal dynamic contact force P' with frequency in Figs 1, 2 and 3. The tangential forces Q'_x and Q'_y respond to fluctuating creepage, i.e. tangential rail *velocities*, and hence show less variation with frequency. Note should be taken of the peak in the lateral and rotational receptances, H_{22} and H_{44}, at 1650 Hz which corresponds to the 'cut-on' at that frequency of the second torsional (web bending) mode of the rail. The oscillating moment caused by the motion of the contact point across the railhead is responsible for the peak in rail rotation at this frequency. This peak is also noticeable in the lateral force spectrum. The small peaks at low frequency are associated with the rail support (pads, sleepers and ballast), as discussed below.

2.1.4 *Conformity*

Conformity influences the behaviour in two significant ways: (a) it increases the spin creepage, which interacts with longitudinal and lateral creepages, and contributes to the frictional power dissipation; (b) it interacts with the lateral and rotational displacements of the rail to cause an oscillating lateral displacement of the contact point. This second effect is best illustrated by Figs 4 and 5, in which the rotations of the rail ϕ, the contact point θ and the input ψ are compared. In Fig. 4 the contact displacement $r\theta$ as a function of frequency is plotted for increasing values of the conformity factor K, at the same reference conditions. It may be seen that the amplitude of the motion increases in direct proportion to K. For all values of K the phase is approximately zero (i.e. in phase with the ripple ψ), except at the two critical frequencies 150 Hz and 1650 Hz.

In Fig. 5 the angle θ/K is compared with the rail rotation ϕ and the input angle ψ (constant at 0.33 mrad). Since the angle α is small, it is possible to approximate equation (24) of the companion paper (**1**) by

$$\frac{\theta}{K} \approx \left(\frac{w_2}{r} - \phi\right) + \psi \tag{1}$$

If the lateral displacement term is also comparatively small, then

$$\frac{\theta}{K} + \phi \approx \psi \tag{2}$$

This is the situation illustrated in Fig. 5, where $\psi = 0.33$ mrad. Torsional oscillation ϕ of the rail is principally excited by the steady normal contact force P_0 acting with a moment arm which oscillates through $\pm r\theta$. The torsional receptance of the rail H_{44} then gives rise to a variation of ϕ with frequency which approximately satisfies equation (2).

2.1.5 *Steady load and friction coefficient*

The normal *dynamic* force depends upon the product of the input displacement Δ and the stiffness of the Hertz spring; it would not be expected to be influenced by the steady

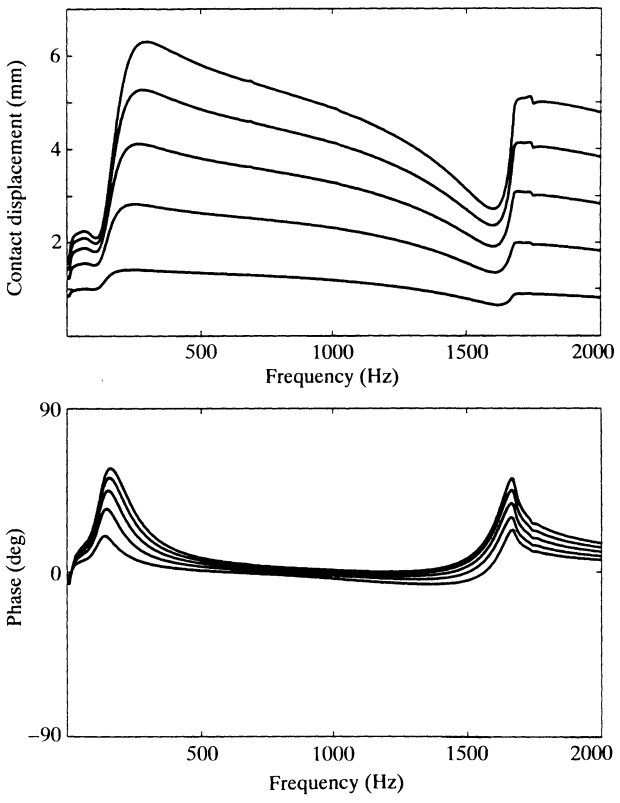

Fig. 4 Effect of conformity factor K on the contact displacement $r\theta$, plotted in amplitude and phase as a function of frequency. Values of K, in order from bottom to top, are 20, 40, 60, 80 and 100

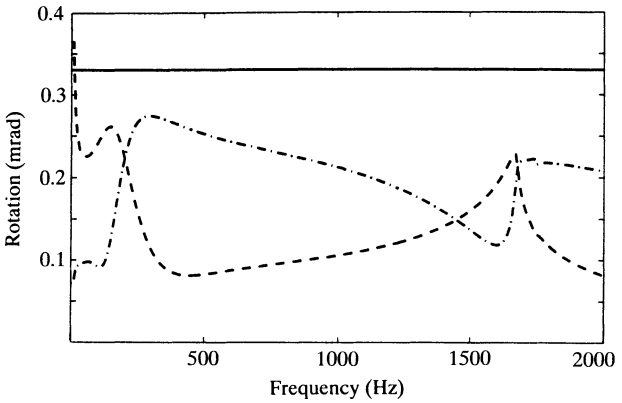

Fig. 5 Variation with frequency of rail rotation and contact displacement, for constant angular input ψ (solid line: input ψ, dashed line: rail rotation ϕ; dash-dot line: θ/K)

load or friction coefficient and that is found to be the case. The increased fluctuating moment due to the steady load causes an increase in rail rotation, but this is offset by the reduction in displacement of the contact point to satisfy equation (2) in subsection 2.1.4.

It follows from equations (19) and (20) of the companion paper (**1**) that the matrix coefficients S_{ij}, which govern the tangential forces Q'_x and Q'_y, scale with μP_0 and the vector $\boldsymbol{s}_i$ scales with $\mu P_0^{4/3}$. Thus Q_x and Q_y increase with P_0 and μ, but as has been seen their effect on rail motion is small. The mean frictional dissipation scales exactly with μP_0; the fluctuating dissipation scales approximately so, the effect being more marked at low frequency than high.

2.1.6 *Steady creepages*

Steady creepages ξ_{x0} and ξ_{y0} can arise from curving, hunting motion or misaligned axles. In a curve the leading axle moves towards the gauge corner of the high rail with an angle of attack which, according to the sign convention in use here [see Fig. 5 of reference (**1**)], corresponds to a *negative* lateral creepage ξ_{y0} at both high and low rail contacts. Equilibrium of the bogie then demands longitudinal creepage ξ_{x0} which is negative (driving) on the high rail and positive (braking) on the low rail. The creepages introduced by misaligned axles in tangent track are comparable (neglecting super-elevation effects) with a curve, the radius of which is such that the angle subtended by the wheel base is equal to the misalignment. (This description is based on analysis of results obtained by British Rail Research, using their program VAMPIRE). Steady creep forces Q_{x0} and Q_{y0} are found from the steady creep equations; they approach saturation under low-spin conditions at a misalignment of about 5 mrad (300 m radius curve). The high spin introduced by close conformity was found to result in $Q_0 \rightarrow \mu P_0$ at creepages of about 0.002.

The principal cause of fluctuating longitudinal creepage was found to be the fluctuation in rolling radius due to the movement $r\theta$ of the contact point [see equation (27) in reference (**1**)], which is almost in phase with the angular ripple ψ at most frequencies. As shown in Fig. 4, this effect increases in proportion to conformity K. For $K = 51$, it gives rise to a maximum oscillating longitudinal force $Q'_0 \approx \pm 7$ kN by the low-spin model (Fig. 1a) and ± 3.5 kN by the high-spin model, at a small lagging phase (Fig. 2a).

Oscillating lateral creep forces are generally smaller in magnitude. They arise mainly from the interactive effect with longitudinal creepage and the small lateral motion of the rail. Steady creepage, in promoting saturation, tends to attenuate the oscillating creep forces Q'_x and Q'_y. Fluctuation in spin creepage arises from changing conicity through θ and a change in contact width b through load.

2.1.7 *Vehicle speed*

Vehicle speed has only a marginal effect on the response of the dynamic model used in this study, whether low- or high-spin contact mechanics are employed, in spite of the factor $(1/V)$ which appears at various points in the contact model. This is because the rail motion and the movement of the contact point $r\theta$ are mainly governed by the input ripple ψ and the moment of the steady load, which are both virtually independent of V. As explained previously, the major oscillating creep force Q'_x is also determined by θ and so is independent of V. Doubling the vehicle speed from 100 to 200 km/h produced no change in rail rotation ϕ, contact displacement $r\theta$ or creep forces. The fluctuating normal contact force P' was increased by about 15 per cent at all frequencies. It is clear, however, from equation (23) of the companion paper (**1**) that the absolute values of all the terms in the expression for power dissipation increase in proportion to V.

2.1.8 *Pad stiffness*

Computer runs were carried out for two different pad stiffnesses, quoted in Table 2 and designated 'hard' and 'soft'. All the results shown in this paper were obtained using the soft pads, except those shown in Fig. 6 where the two pad stiffnesses were compared. As can be seen

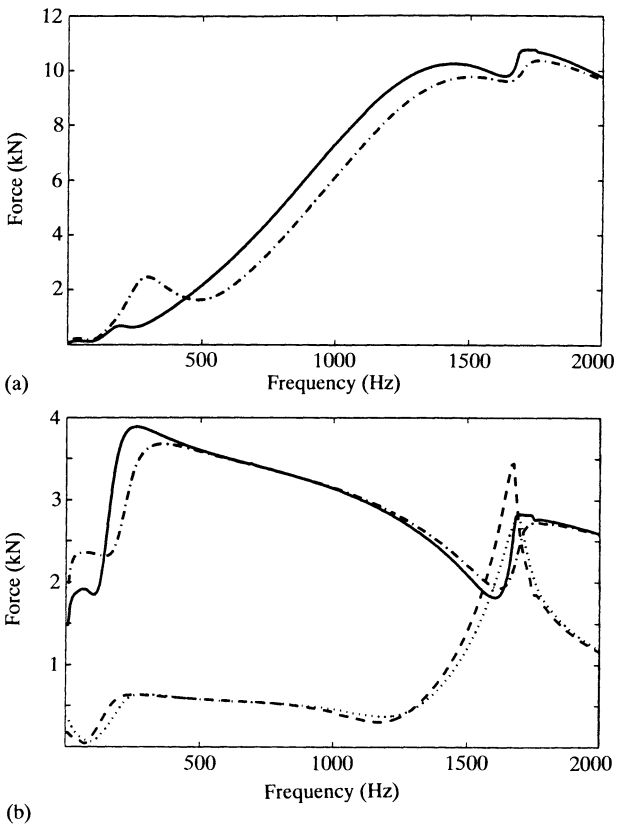

Fig. 6 Effect of rail pad stiffness on contact forces: (a) normal force P' (solid line: soft pads, dash-dot line: hard pads); (b) tangential forces (solid line: Q_x soft pads, dash-dot line: Q_x hard pads, dashed line: Q_y soft pads; dotted line: Q_y hard pads)

from Fig. 6, the pad stiffness influences the contact forces only in the low-frequency regime, less than 400 Hz or so. Two well-damped resonances to vertical excitation can be identified at low frequency: one at about 100 Hz is governed by the ballast stiffness; the other is a resonance of the sleeper on the stiffness of the pad. For the soft pads this occurs at about 180 Hz and for the hard pads at about 300 Hz. At this resonance the amplitude of normal contact force P' is increased threefold by the hard pad. The effect of pad stiffness on tangential forces is insignificant.

2.1.9 *Frictional energy dissipation*

According to the Frederick–Valdivia theory of corrugation development, surface irregularities either grow or are suppressed according to whether the real part of the oscillating component of the frictional energy dissipation W' is negative or positive (since the imposed 'ripple' Δ has been defined to be positive for a corrugation crest on the railhead, negative for a trough). The expression for W' is given in equation (23) of the companion paper (**1**). It comprises six complex terms: the steady forces and spin moment acting through the oscillatory creepages and the oscillating forces and moment acting through the steady creepages. The phase of the resultant is not easy to predict by purely qualitative arguments. However, by extracting the values of the separate terms at a representative frequency for a variety of parametric conditions, it has been possible to make some tentative statements.

Of all the cases examined the most significant difference occurs between those in which the rotational ripple $\psi \neq 0$ (generally 0.33 mrad) and those in which $\psi = 0$. In the former cases the term $M_{z0}/R_1 \cos(\lambda + \alpha)\theta$ is dominant, i.e. the steady (mean) spin moment acting through the oscillating spin creepage. As explained previously, the oscillating spin creepage, which increases with conformity, is roughly in phase with the ripple, ensuring that this term always has a positive real part. Its magnitude is such that, in nearly all cases where $\psi \neq 0$, the resulting dissipation is positive, leading to the attenuation by wear of the pre-existing ripple.

It is instructive to consider the other terms in the expression for W. It has been seen that ξ'_x is composed largely of v''_x/V given by equation (27) of reference (**1**), which is always negative, hence Q'_x is always positive. This means that the signs of the terms $Q_{x0}\xi'_x$ and $Q'_x\xi_{x0}$ depend upon the sign of ξ_{x0}; if ξ_{x0} is positive, Q_{x0} is negative and both terms are positive, contributing to a negative value of W. The reverse is true if ξ_{x0} is negative. On the other hand the term $Q_y\xi'_y$ is negative whatever the sign of ξ_{y0}, thereby contributing to a positive value of W. The term $Q'_y\xi_{y0}$ is generally found to be small.

The overall implications of conformity for corrugation growth, within this linear wear model, may best be brought out by a new way of displaying the results of computations. Since for any given case, interest is centred on a single function of frequency (the real part of the fluctuating energy dissipation), the functional dependence on the conformity factor K can be represented in a single plot. Figure 7a shows the variation of this function with both frequency and K, for conditions corresponding to Fig. 2.

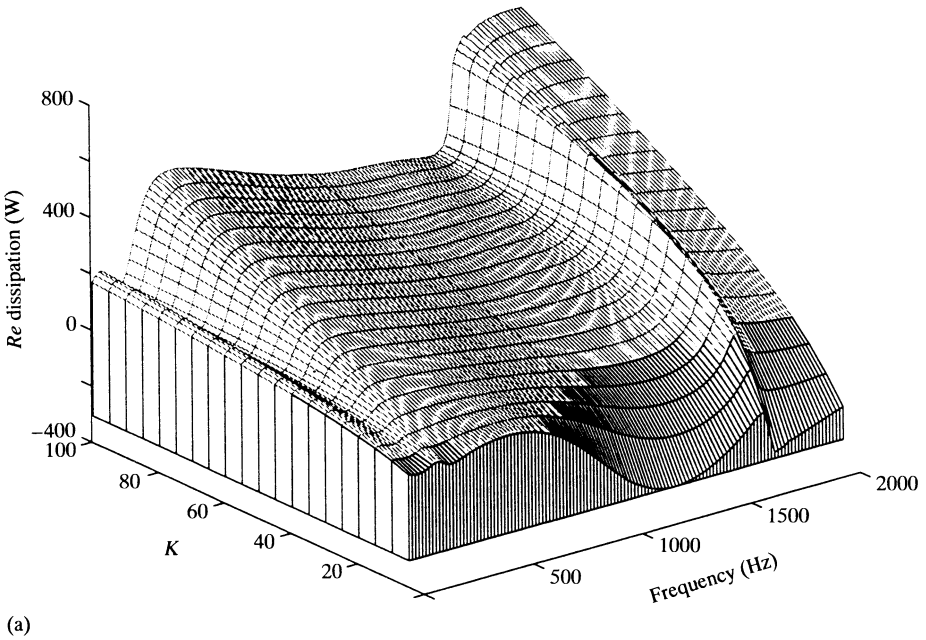

(a)

Fig. 7 Effect of conformity on frictional energy dissipation: (a) for conditions as in Fig. 2; (b) for conditions as in Fig. 3; (c) for conditions as in (b) but with imposed lateral creepage reduced by a factor 5

The surface is plotted in darker lines where the function is negative, corresponding to corrugation growth, and in lighter lines where corrugations will attenuate. What is revealed is that growth is only predicted for rather low conformity, and mainly for relatively high frequencies. As conformity increases, the function grows increasingly positive at all frequencies, so that corrugation growth tends to be suppressed.

When the rotational component of the input ripple is suppressed, the picture is rather different. Figure 7b shows a corresponding plot for the case in which all that has been changed is that ψ has been set to zero. The strongest 'deepening' action is still predicted in much the same region of the diagram, but now for frequencies up to 1200 Hz or so the function does not increase with conformity, but remains close to zero over the whole range considered. If the assumed steady lateral creepage (arising from an assumed misalignment of the wheel on the rail) is reduced by a factor of 5, the results change a little to what is plotted in Fig. 7c. The strong 'deepening' action at low conformity and high frequency has now vanished, and there is a small but systematic tendency toward progressively stronger deepening as conformity increases, strongest around 800 Hz, a rather typical corrugation frequency. This

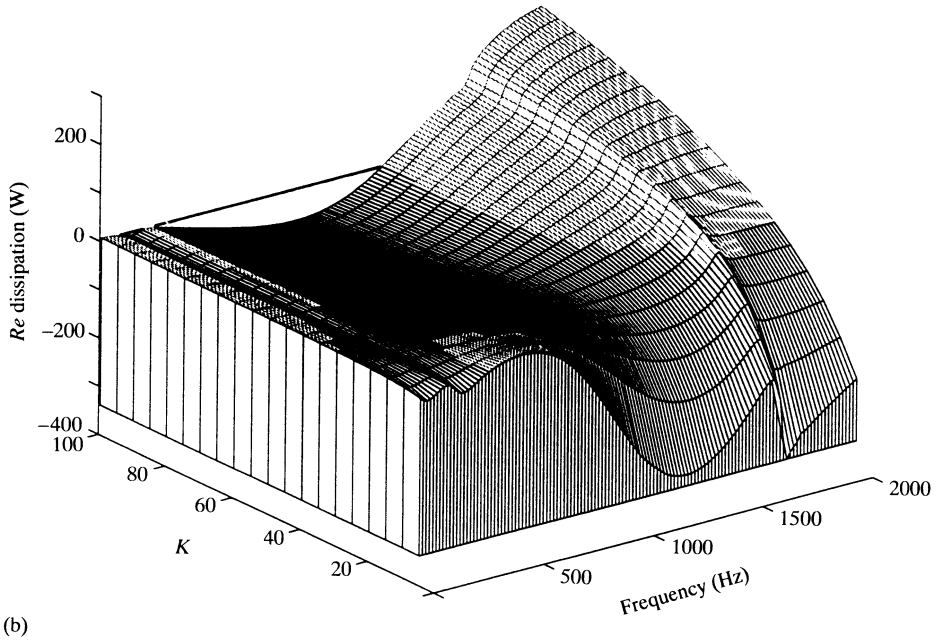

(b)

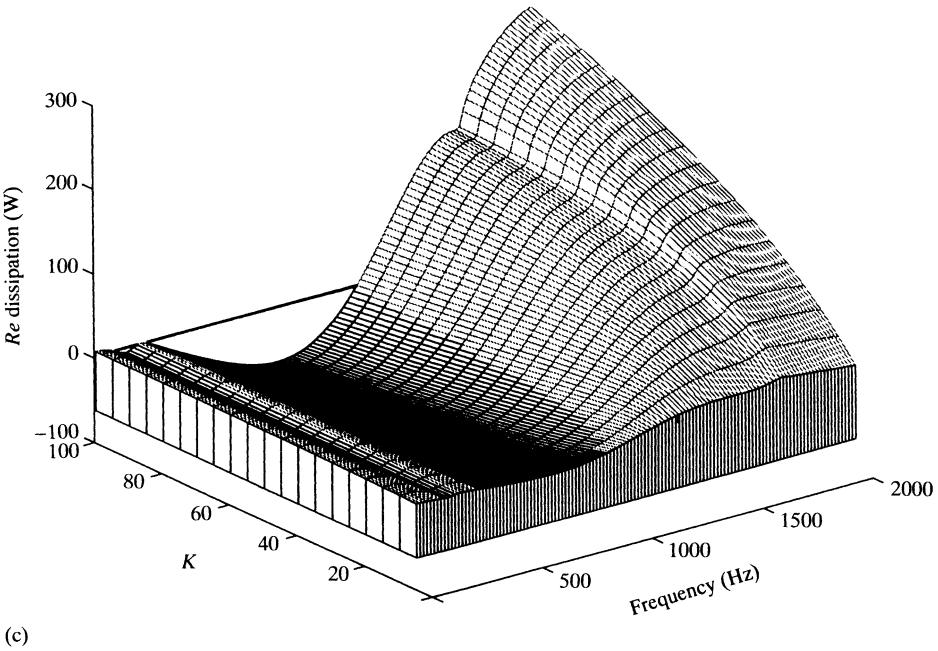

(c)

Fig. 7 (*continued*)

last finding may be compared with that of Hempelmann and Knothe (**2**), who found, with low conformity, normal excitation and rather small lateral creepage only, that W exhibited a negative real part over a wide range of conditions and frequency, and that the values increased with conformity.

In summary, conformity has a significant influence on the tendency to deepen or to erase pre-existing rail/wheel roughness. The details, and even the sign of the change with conformity factor K, vary for different assumed running conditions, and such variations should certainly be taken into account in any analysis.

2.2 Two-point contact

The two-point contact model differs from the single-point model in that the two contacts are assumed to be circular and not to move laterally across the railhead. It is therefore appropriate to use the low-spin creepage model for each contact point; large-scale spin creepage for the 'conformal contact' is taken into account by a fixed difference in longitudinal creepage between the two points, the magnitude of which depends upon their spacing AC and BC as shown in Fig. 9 of reference (**1**). Independent input ripples $\Delta_A e^{i\omega t}$ and $\Delta_B e^{i\omega t}$ are applied at the two points of contact A and B. Output quantities were chosen to be the dynamic rail displacements w_2, w_3 and ϕ; the dynamic contact forces Q'_x, Q'_y and P', and the frictional power dissipation at each point of contact W_A and W_B. Note that the dissipation is perhaps modelled more accurately within this model than in either of the single-point contact models: the effects both of transient creepage and of spin dissipation are now allowed for, whereas the two previous models each allowed for one of these effects but not the other.

2.2.1 Comparison with single-point contact

First, the two-point program was run for conditions comparable to those for the single point of contact shown in Fig. 2, by setting $(\Delta_A + \Delta_B)/2 = \Delta = 5.01 \times 10^{-6}$ m and $(\Delta_B - \Delta_A)/AB = \psi = 3.27 \times 10^{-4}$ rad. The contact positions were chosen such that AC $= -10$ mm; BC $= 20$ mm. Half the total load of 50 kN was assumed to be carried by each point of contact. The output is displayed in Fig. 8. Comparing Fig. 8a with Fig. 2b (with allowance for the change of scale) shows that the rail displacements and rotations are almost identical for one- or two-point contacts. Whereas the single point responds to the rotation of the rail by displacing laterally, the two fixed points experience oscillating normal loads P'_A and P'_B of magnitude about 4 kN which are about 180° out of phase. The fluctuating tangential contact forces are somewhat smaller (about 1.0 kN) than in the single-point case. Both the mean and fluctuating total energy dissipation are of similar magnitude for one- and two-point contact, but this depends on the choice of contact positions A and B.

This degree of agreement between the independent models is very encouraging in terms of cross-checking both the physical modelling processes and the computer implementations.

2.2.2 Input ripple

Cases have been run in which either $\Delta = 0$ or $\psi = 0$. The effect is as expected. When $\Delta = 0$ ($\Delta_B = -\Delta_A$) the vertical motion of the rail is negligible and the oscillating contact forces P'_A and P'_B are about ± 3 kN and 180° out of phase. When $\psi = 0$ ($\Delta_B = \Delta_A$) the rotation of the rail is small; $P'_A \approx P'_B$ and are in phase. The tangential forces are similar in magnitude to those shown in Fig. 8b.

When the cases with $\Delta = 0$ or $\psi = 0$ are examined separately, a useful physical simplification is revealed for which there is no direct parallel in the single-point contact model. The maximum spacing of the points A and B which could reasonably occur in practice is of the order of 30 mm. For this spacing, and using the known stiffness of the Hertz springs at A and B and the typical values of the vertical and rotational rail receptances, it is easy to demonstrate that for pure vertical input (i.e. $\psi = 0$) there is little compression of the Hertz springs so that the input ripple is mainly taken up in vertical rail motion, whereas for purely rotational input (i.e. $\Delta = 0$) the opposite happens: the input is taken up primarily in the Hertz springs, and relatively little rotation of the rail is caused.

2.2.3 Steady creepage

Fluctuations in creepage and tangential forces in the two-point case arise principally from fluctuations in the contact loads P'_A and P'_B which, provided $\psi \neq 0$, are out of phase. The effect of spin is to introduce longitudinal creepages, positive at A and negative at B. If P'_A is positive it will increase the positive creepage at A, and P'_B then being negative will reduce the negative creepage at B. Thus the *changes* in creepage at A and B, and the resulting changes in creep forces, will all be positive. The addition of a steady longitudinal creepage $\pm\xi_{x0}$ increases the force Q'_x at one point of contact and reduces it at the other. A steady lateral creepage ξ_{y0}, on the other hand, is equal at A and B so that the fluctuating lateral forces Q'_y are out of phase at A and B and change sign with a change in sign of ξ_{y0}.

2.2.4 Frictional power dissipation and wear eigenvalues

If the two points of contact A and B are subjected to harmonic input ripples Δ_A and Δ_B of the same frequency ω and arbitrary phase, the frictional energy dissipation rates at A and B satisfy a relation

$$\begin{bmatrix} W_A(\omega) \\ W_B(\omega) \end{bmatrix} = \begin{bmatrix} P_{11}(\omega) & P_{12}(\omega) \\ P_{21}(\omega) & P_{22}(\omega) \end{bmatrix} \begin{bmatrix} \Delta_A \\ \Delta_B \end{bmatrix} \tag{3}$$

The frequency dependent coefficients P_{ij} can be found, for

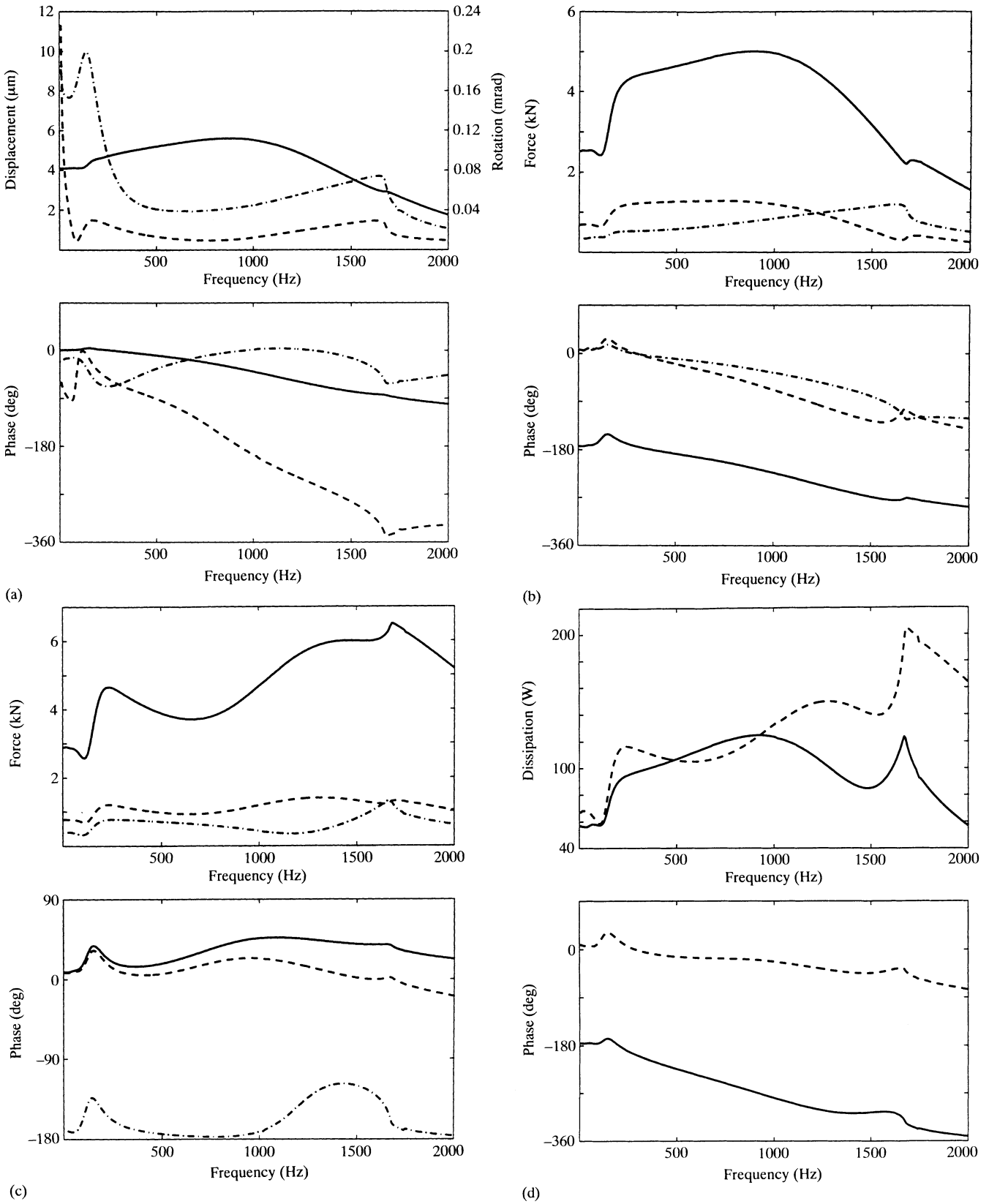

Fig. 8 Results for the two-point contact model, for comparable input parameters to those of Figs 1 and 2: (a) rail displacements (solid line: vertical, dashed line: horizontal) and rotation (dash-dot line); (b) contact forces at point A (solid line: P', dashed line: Q_x, dash-dot line: Q_y); (c) contact forces at point B (solid line: P', dashed line: Q_x, dash-dot line: Q_y); (d) frictional power dissipation at points A (solid line) and B (dashed line)

any given operating conditions, by computing separately the cases $\Delta_A = 1$, $\Delta_B = 0$ and $\Delta_A = 0$, $\Delta_B = 1$. Suppose this 2×2 matrix has eigenvalues λ_1, λ_2 and corresponding eigenvectors $\boldsymbol{u}_1$, $\boldsymbol{u}_2$. Then the vector of input ripples may be expressed as

$$\Delta = \alpha \boldsymbol{u}_1 + \beta \boldsymbol{u}_2 \tag{4}$$

and the Frederick–Valdivia wear takes the form

$$\dot{\alpha} = -\chi \lambda_1 \alpha, \qquad \dot{\beta} = -\chi \lambda_2 \beta \tag{5}$$

where the positive constant χ relates energy dissipation to wear rate. It is immediately apparent that the long-term wear behaviour is dominated by the faster growing (or slower decaying) eigenvalue, i.e. the one of λ_1, λ_2 with the lesser real part.

The eigenvalues and eigenvector ratios Δ_A: Δ_B for a typical case are shown in Figs 9 and 10. Note first from Fig. 10 that, up to a frequency of 1000 Hz the magnitude $|\Delta_A$: $\Delta_B|$ for both modes is about unity, while the relative phase is about 0° in one mode and 180° in the other. Thus, in this frequency range, one mode is almost pure displacement (broken line) and the other pure rotation (solid line). Turning to the eigenvalues in Fig. 9, the displacement mode has a positive real part over the whole frequency range, corresponding to wearing out of an initial ripple, although

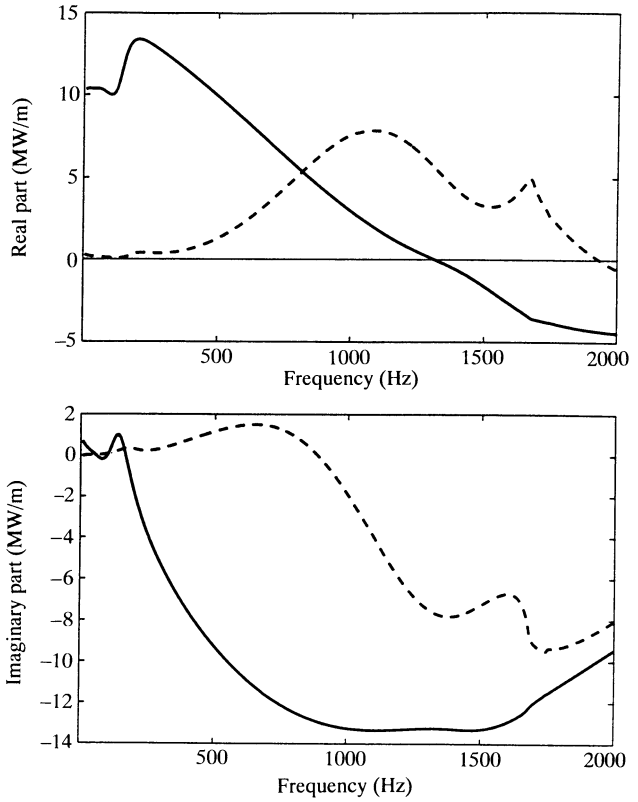

Fig. 9 Two-point contact, eigenvalues λ_1, λ_2 of the matrix of equation (3)

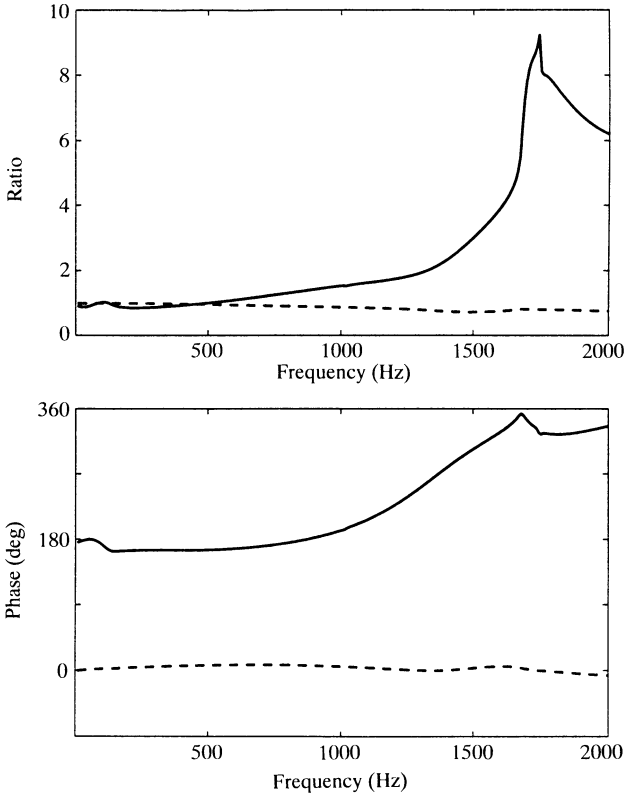

Fig. 10 Eigenvector ratios Δ_A: Δ_B corresponding to the eigenvalues plotted in Fig. 9

at a low rate of wear at low frequency. The rotation mode has large positive values at low frequency, but becomes negative, corresponding to corrugation growth, above 1300 Hz.

The single-point-of-contact model, in either the low-spin or high-spin formulation, does not lend itself easily to similar treatment. Close conformity leads to a wide, thin contact ellipse, of semi-width $b = 20$ and 26 mm in the cases examined above ($K = 21$ and $K = 51$). With rotational input ($\Delta = 0$, $\psi = 0.33$ mrad) the contact patch oscillates across the railhead (Fig. 4) with an amplitude 1.5 mm ($K = 21$) and 3.5 mm ($K = 51$). In these circumstances the frictional energy dissipation is found to have a large positive real part, tending to suppress corrugation growth. On the other hand, with a purely displacement input ($\Delta = 5.0$ μm, $\psi = 0$), the amplitude of the lateral motion of the contact area is less than 0.1 mm and the phase of the frictional energy dissipation fluctuates in the neighbourhood of 90°, leading to a translation of the ripple along the rail without change of amplitude.

The wear mode analysis of two-point contact suggests that the wear modes approximate, over a substantial frequency range, to pure rotation and pure displacement. Assuming this to remain true for one-point contact, it is possible to conclude that rotational ripples will be suppressed, but that normal displacement ripples are approximately in neutral equilibrium.

3 CONCLUSIONS

The high-frequency dynamic behaviour of a closely conforming wheel–rail contact has been examined. Close conformity between the transverse profiles of the wheel and rail gives rise to a wide contact patch, which leads to a large spin creepage through the large difference in rolling radius across the width of the patch. The spin creepage profoundly influences the contact mechanics. Three new contact mechanics models have been developed in the companion paper (**1**); two of them include the large spin effect:

(a) linear interactive longitudinal and lateral creepage model, including transient creepage effects but including linear spin creepage only; applicable to low–moderate spin creepage;
(b) full slip model with interactive longitudinal, lateral and spin creepage; applicable to high spin; and
(c) linear two-point contact model in which spin is manifested by equal and opposite longitudinal creepage at each point of contact, modelled separately using case (a).

A single closely conforming contact responds to lateral and rotational oscillations of the rail by relatively large lateral oscillations of the contact point. A two-point contact responds by large fluctuations of the normal forces at the two points of contact. The combination of the dynamic model of the rail with the contact mechanics gives a closed-loop system: oscillations of the rail lead to oscillatory creepage, which causes oscillatory contact forces which, in turn, feed back to excite vibration of the rail. The dynamic stability of this closed-loop system has been examined. The system has been found to be stable, with either single- or two-point contact, for all degrees of conformity and for all conditions of steady running. Thus no self-excited oscillations of the vehicle hunting type would be expected within this model.

In the present paper, the forced response of the system to surface irregularities has been investigated, using all three contact models. The influence has been discussed of a wide range of parameters: frequency, conformity, steady creepages, load, friction coefficient, rail-pad stiffness and vehicle speed. The input comprised an independent combination of a sinusoidal normal displacement $\Delta\, e^{i\omega t}$ and a rotation $\psi\, e^{i\omega t}$. For a given set of input parameters all three contact models predicted broadly the same motion of the rail and normal contact forces. The low-spin model (a) underestimates the frictional power dissipation; the high-spin model (b) probably overestimates it somewhat, and underestimates the tangential contact forces. The two-point contact analysis is likely to be the most accurate, although it only describes a rather extreme case.

The response to Δ and ψ was significantly different. With a rotational input ψ the rail oscillated in torsion, which caused a single point to oscillate across the railhead and gave rise to large fluctuations in contact force of opposite phase at two points of contact. These did not occur with a non-rotational input. An eigenvalue analysis of two-point contact has shown that in the frequency range 0–1000 Hz the independent (i.e. normal) modes of wear are close to pure displacement ($\psi = 0$) and pure rotation ($\Delta = 0$).

The frequency response of the system is relatively simple. With a continuous support rail model only three peaks were observed: two occur at low frequency (below 350 Hz) and are associated with the ballast and the pads, and the third occurs at about 1650 Hz and is associated with a second torsional (web bending) propagation mode for waves on the rail. With a constant input the normal contact forces increase with frequency in accordance with the decrease in vertical receptance of the rail. The tangential contact forces, which are governed by creepage, do not vary much with frequency.

The effect of other parameters, such as load, friction coefficient and vehicle speed, had only a small or predictable effect on the response of the system. In particular, the stiffness of the rail pads only influences the behaviour significantly at frequencies which are rather low for short-pitch corrugation phenomena under typical Intercity operating conditions.

According to the Frederick–Valdivia hypothesis, corrugation initiation is determined by the phase of the fluctuating frictional power dissipation relative to the input ripple: a negative real part corresponds to the ripple being deepened by wear, i.e. corrugation growth; a positive real part corresponds to the input ripple being worn flat. It is one of the most significant conclusions of this investigation that in conditions of close conformity, producing high-spin creepage, the frictional power tended to be positive, leading to the suppression of corrugation growth. This was found to be the case with both single- and two-point contact. Only with zero rotational input, under conditions similar to those investigated by Hempelmann and Knothe (**2**), could significant enhancement of corrugation growth be predicted from increased conformity. Ripples which generate rotational motion ($\psi \neq 0$) are found to be suppressed except for higher frequencies (above 1300 Hz).

4 IMPLICATIONS FOR CORRUGATION RESEARCH

It must be admitted that the conclusions of this investigation, summarized in the previous section, are largely negative from the point of view of explaining Kalousek's observations of the effect of conformity in promoting corrugations on the Vancouver 'Skytrain', having a characteristic relationship between wavelength and speed (**3**). These observations remain to be explained in a satisfactory way, and further study will be required.

The present investigation also suggests that high spin associated with close conformity significantly alters the rate of corrugation growth according to the Frederick–

Valdivia hypothesis. Differential roughness across the width of the rail or wheel tread, leading to rotational input, tends to be suppressed ever more strongly as conformity increases, while vertical input may be suppressed or enhanced, in a way which may either increase or decrease with increasing conformity, depending on the detailed running conditions of the wheel on the rail. For this conclusion to be investigated in more detail, a rail model with discrete supports should be used in conjunction with an interactive contact model such as the authors have used, so that the 'pinned–pinned' anti-resonances are included. However, a predicted critical dependence on these anti-resonance frequencies would not help to explain the situation in Vancouver, where the corrugation wavelength was observed to be independent of support spacing.

With these considerations in mind it is suggested that effects not included in the present models would merit further investigation. An obvious possibility is to include the effects of wheel resonances in the model—these seem unpromising in so far as they occur at particular, rather well-defined, frequencies, but wheel deformation does offer the possibility of storing some elastic energy which might be recovered at another part of the oscillation cycle, perhaps allowing unstable oscillation to arise in a self-excited manner. Another possibility would be to carry out non-linear computations in the time domain, which would permit a direct investigation of possible roll–slip oscillations (which had been suggested by the observations in Vancouver). The negative conclusion of the stability analysis reported here does not promise well for such an investigation, but perhaps in conjunction with other enhancements to the models self-sustained roll–slip oscillation will be found to be possible under certain operating conditions.

ACKNOWLEDGEMENTS

The authors are pleased to acknowledge assistance with the work reported here. Graham Scott of British Rail Research performed creepage calculations on bogies with misaligned axles to provide input for this study. This work was carried out with financial support from ERRI Committee D185 through BR Research.

REFERENCES

1 **Bhaskar, A., Johnson, K. L., Wood, G. D.** and **Woodhouse, J.** Wheel–rail dynamics with closely conformal contact Part 1: dynamic modelling and stability analysis. *Proc. Instn Mech. Engrs, Part F,* 1997, **211** (F1), 11–26.

2 **Hempelmann, K.** and **Knothe, K.** An extended linear model for the prediction of short wavelength corrugation. *Wear*, 1996, **191**, 161–169.

3 **Kalousek, J.** and **Johnson, K. L.** An investigation of short pitch wheel and rail corrugation on the Vancouver mass transit system. *Proc. Instn Mech. Engrs, Part F*, 1992, **206**, 127–135.

4 **Valdivia, A.** The interaction between high-frequency wheel–rail dynamics and irregular rail wear. *VDI-Fortschrittsbericht*, Reihe 12, Nr. 93, 1988, Dusseldorf.

5 **Frederick, C. O.** A rail corrugation theory. Proceedings of the 2nd International Conference on *Contact Mechanics of Rail/wheel Systems*, University of Rhode Island, 1986, pp. 181–211 (University of Waterloo Press).